Peptide Science 2011: K. Sakaguchi (Ed.)
The Japanese Peptide Society (2012)

A Novel Modification Method of Peptides and Proteins by Anionic Dodecaborate Cage in Water

Yoshihide Hattori[1], Yuko Katsuta[1], Mari Mukumoto[1], Kouki Uehara[2], Youichirou Ohta[2], Tomoyuki Asano[2], Minoru Suzuki[3], Shin-ichiro Masunaga[3], Koji Ono[3], Shinji Tanimori[1], and Mitsunori Kirihata[1]

[1]Department of Bioscience and Informatics, Graduate School of Life and Environmental Sciences, Osaka Prefecture University, 1-1 Gakuen-cho, Nakaku, Sakai, Japan, [2]Stella Pharma Co., ORIX Kouraibashi Bldg. 5F, 3-2-7 Kouraibashi, Chuo-ku, Osaka, Japan, and [3]Kyoto University Research Reactor Institute, 2, Asashiro-Nishi, Kumatori-cho, Sennan-gun, Osaka, Japan
e-mail: y0shi_hattori@riast.osakafu-u.ac.jp

In order to conduct the thiododecaborate (-S-$[B_{12}H_{11}]^{2-}$) unit to the residual thiol groups on target peptides by coupling reaction under aqueous conditions, we have newly devised two modification reagents BSH-Npys (2) and BSH-DNpys (3). The synthesis of thiododecaborate-containing glutathione (4) and its analogues (5, 6) by use of 2 and 3, and biological evaluation in vitro as boron agent for BNCT were described.

Keywords: boron agent for BNCT, boron cage peptide, mercaptoundecahydro-*closo*-dodecaborate (BSH), thiododecaborate-containing peptide

Introduction

The boron cluster compounds comprised of anionic dodecaborate cage $[B_{12}H_{12}]^{2-}$ are particularly interesting molecule, because they have characteristic regular icosahedral structure and unique chemical and biological properties. Recently, many application studies of dodecaborate cage focused on their intrinsic properties are currently progressed in the various fields. One of the important applications of dodecaborate compounds is related to boron agent for boron neutron capture therapy (BNCT) for cancer. In particular, mercaptoundecahydro-*closo*-dodecaborate (BSH, $[B_{12}H_{12}]^{2-}SH$, **1**) in which boron atoms are enriched with ^{10}B isotope has been used clinically for the treatment of patients with malignant brain tumor by BNCT.

BNCT is based on the nuclear reaction of ^{10}B with thermal/epithermal neutrons to yield high linear energy transfer α particles (^{4}He) and recoiling ^{7}Li nuclei in tumor

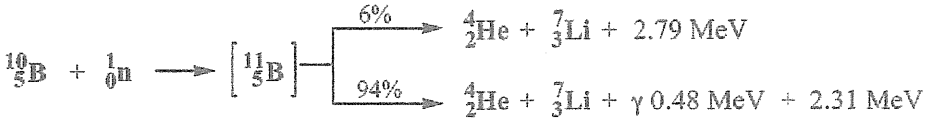

Fig. 1. Two Parallel Nuclear Fission between Neutron and ^{10}B Nucleus.

cells (Fig. 1) [1]. For a boron delivery agent to be successful in BNCT, the following criteria must be met: i) high tumor targeting selectivity (T/N >3-4:1); ii) low systemic toxicity; iii) tumor concentrations of ~ 20 μg ^{10}B /g tumor tissues. Over the past 20 years, various boron carrier molecules such as amino acids, nucleic acids and liposomes etc. have been designed and synthesized [2].

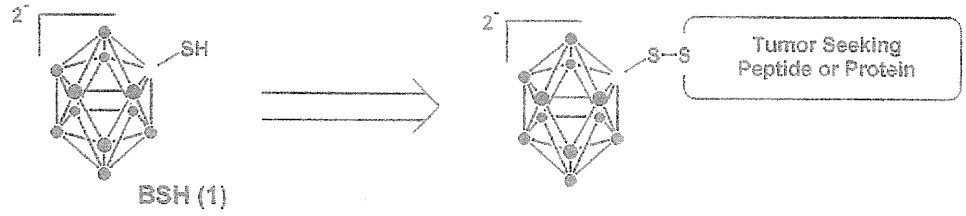

Fig. 2. Design Concept of Boron Agent for BNCT.

Our strategy for attaining the required concentration is to design the tumor seeking peptides or proteins such as antibodies bearing large number of polyhedral boron cages (Fig. 2). In the present study, we have adopted anionic thiododecaborate ($-S[B_{12}H_{12}]^{2-}$) unit linked to residual thiol groups on peptides or proteins by forming disulfide like (B-S-S-C) bonds, and also newly developed two modification reagents in order to conduct the unit to thiol groups.

We now described a new conjugation method of thiododecaborate unit to the thiol group on glutathione (GSH) and it's analogues used as a model peptide, and also their biological evaluation as boron agent for BNCT.

Results and Discussion

Preparation of Modification Reagents, BSH-Npys (2) and BSH-DNpys (3)

Two kinds of reagents (**2** and **3**) bearing nitropyridyl group for conjugation of thiododecabarate unit to thiol group were synthesized by the reaction of BSH·2Cs with nitro/dinitro-pyridylsulfenyl chloride as pure state in moderate yield, respectively, as shown in Fig. 3.

Synthesis of Thiododecaborate-Containing Peptides (Thiododecaboration of Thiol Group)

The coupling reaction of GSH with **2** in aqueous solution was required long reaction time (over 3 days) to give GSH-BSH (**4**), and the isolation yield of disulfide **4** was slight low owing to by-production of GSH-dimer *in situ*. In contrast, the same coupling of GSH with **3** was furnished within 30 min to afford **4** in 81% isolation yield without any formation of BSH-dimer (Fig. 4). These results demonstrated BSH-DNpys **3** to be more suitable for the synthesis of thiododecaborate-contaning peptide. This reaction was applied to case of cystein-containing dipeptides, CysGly and CysVal, to give the corresponding CysGly-BSH (**5**) and CysVal-BSH (**6**), respectively, in good yield as shown in Fig. 5.

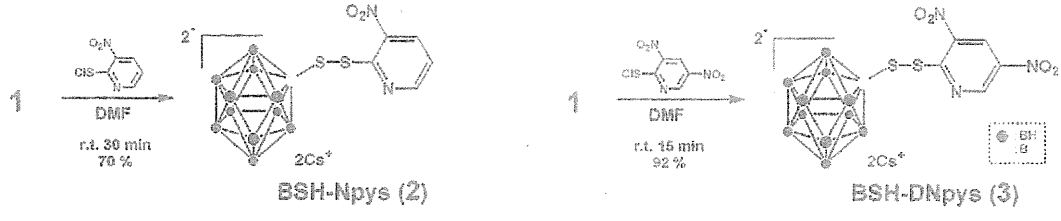

Fig. 3. Preparation of Modification Reagents 2 and 3.

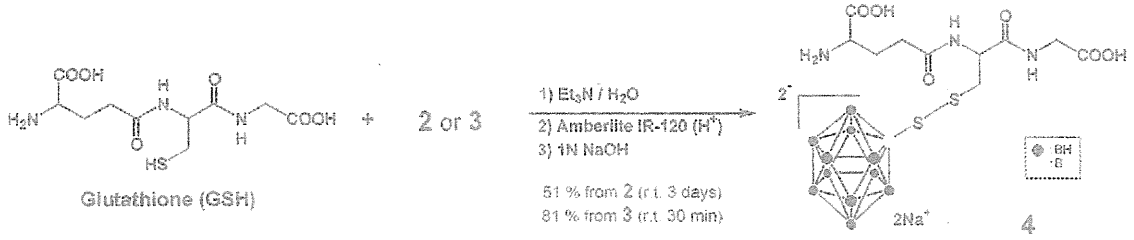

Fig. 4. Synthesis of Thiododecaborate-Containing GSH.

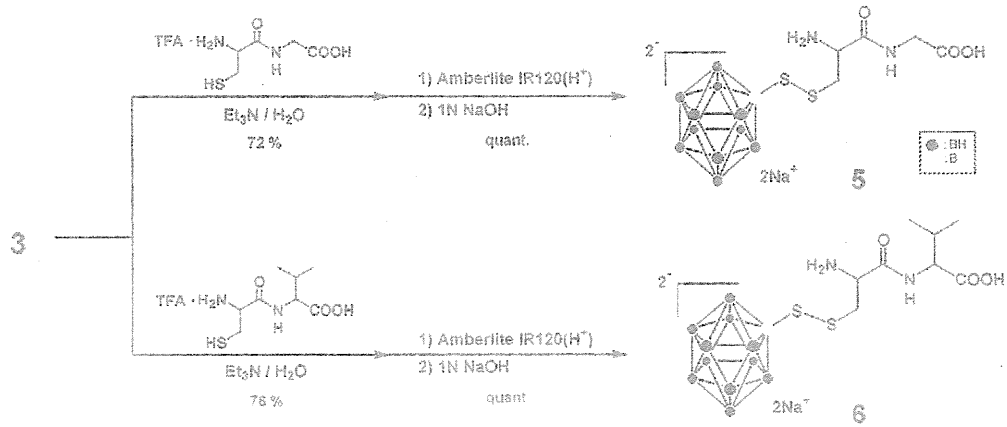

Fig. 5. Synthesis of Thiododecaborate-Containing Dipeptides.

Boron Uptake Study

To evaluate thiodecaborate-containing peptides **4-6** as boron agent for BNCT, we examined the boron uptake test using B16 (mouse melanoma) and C6 (mouse glioma) cells *in vitro*. The intracellular boron concentration was measured by inductively coupled plasma atomic emission spectroscopy (ICP-AES) technique. The boron concentrations of **4-6** in both cancer cells were higher than that of L-Boronophenylalanine (BPA) as of positive control substance, which was clinically used as boron agent in cure of cancer by BNCT (Fig. 5).

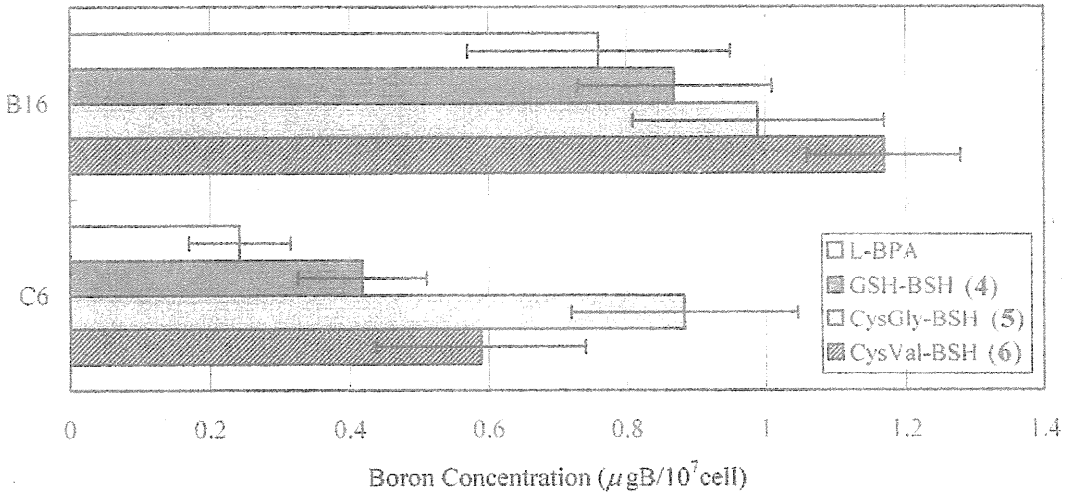

Fig. 6. Boron Concentration in B16 and C6 cells.

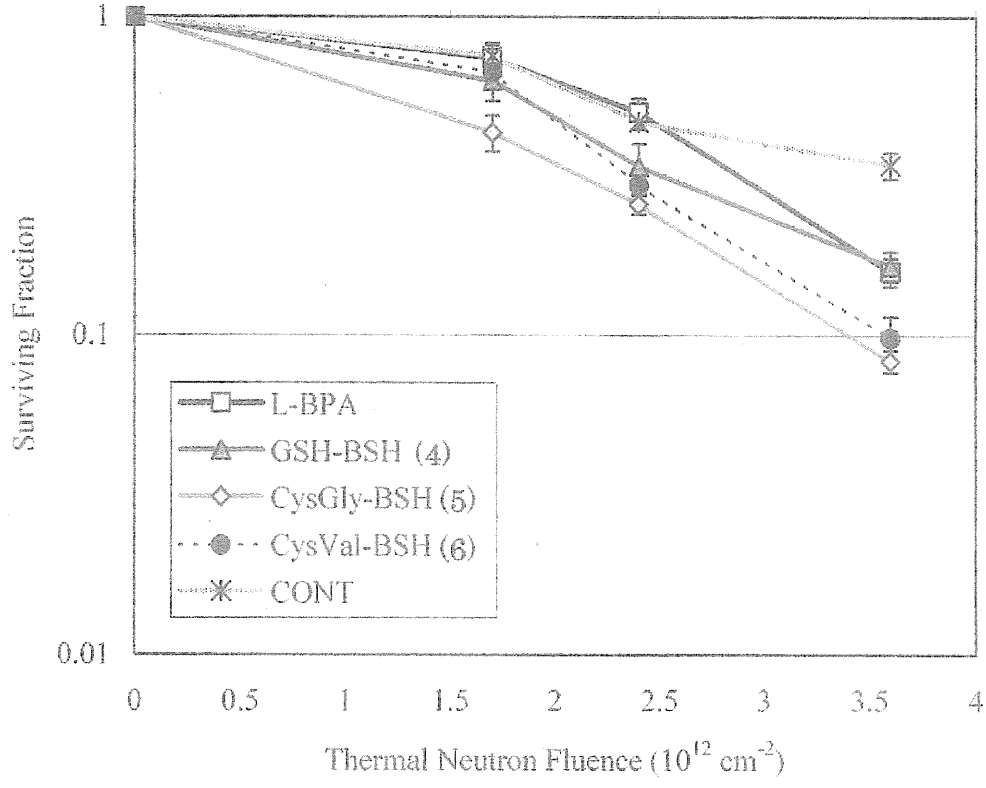

Fig. 7. Killing Effects by Neutron Irradiation Toward B16 Cell.

Killing Effect by Neutron Irradiation

Fig. 7 showed *in vitro* killing effects of peptides **4-6** toward B16 cell by neutron irradiation. Among these peptides, CysGly-BSH (**5**) showed the strongest killing effect in spite of its boron uptake was lower than **6**. Killing effects assay using another kind of cancer cell and mouse bearing cancer are currently in progress.

In conclusion, we accomplished the conductive method of thiododecaborate unit to the residual thiol groups on peptide in water by using of newly developed modification reagents, and also the biological activities of thiododecaborate-containing peptides synthesized here were evaluated. These thiododecaborate-containing peptides might be potentially useful in treating cancer by means of BNCT.

References

1. Barth, R. F.; Coderre, J. A.; Vicente, M. G.; Blue, T. E. (2005) *Cancer Res.*, **11**, 3987-4002.
2. Soloway, A. H.; Tjarks, W.; Barnum, B. A.; Rong, F. G.; Barth, R. F.; Codogni, I. M.; Wilson, J. G. (1998) *Chem. Rev.*, **98**, 1515–1562.

Peptide Science 2011: K. Sakaguchi (Ed.)
The Japanese Peptide Society (2012)

Dodecaborate-Containing L-Amino Acids as New Boron Carriers for Boron Neutron Capture Therapy

Yoshihide Hattori[1], Shintarou Kusaka[1], Mari Mukumoto[1], Kouki Uehara[2], Youichirou Ohta[2], Tomoyuki Asano[2], Minoru Suzuki[3], Shin-ichiro Masunaga[3], Koji Ono[3], Shinji Tanimori[1], and Mitsunori Kirihata[1]

[1]Department of Bioscience and Informatics, Graduate School of Life and Environmental Sciences, Osaka Prefecture University, 1-1 Gakuen-cho, Nakaku, Sakai, Japan, [2]Stella Pharma Co., ORIX Kouraibashi Bldg. 5F, 3-2-7 Kouraibashi, Chuo-ku, Osaka, Japan, and [3]Kyoto University Research Reactor Institute, 2, Asashiro-Nishi, Kumatori-cho, Sennan-gun, Osaka, Japan
e-mail: y0shi_hattori@riast.osakafu-u.ac.jp

A convenient and simple synthetic method of thiododecaborate- ($[B_{12}H_{11}]^{2-}$-S-) unit-containing L-α-amino acid, a new class of boron carrier for BNCT, was accomplished from BSH derivative and ω-bromo-L-α-amino acids by nearly one step S-alkylation. In the present paper, the synthesis and biological evaluation of new -thiododecaborate -L-amino acids are described.

Keywords: boron cage amino acid, boron carrier for BNCT, BSH-L-amino acid, L-amino acid, thiododecaborate-containing

Introduction

Although many kinds of boron compounds such as amino acid, nucleic acid and liposome have been reported as boron delivery agent (boron carrier) for boron neutron capture therapy (BNCT), only two compounds, *p*-borono-L-phenylalanine (BPA) and mercapto-*closo*-undecahydrododecaborate (BSH) of them, are clinically used in cure of cancer with BNCT. For a boron delivery agent to be successful in BNCT, the following criteria must be met: i) high tumor targeting selectivity (T/N >3-4:1); ii) low systemic toxicity; iii) tumor concentrations of ~ 20 μg ^{10}B/g tumor tissues, iv) high water solubility. On the other hand, the L-amino acid transport system in tumor cell is enhanced to guarantee the cell multiplication, compared with normal tissues [1]. Therefore, there has been a long-standing interest on the design, synthesis and biological evaluation of boron-containing α-amino acid having tumor seeking and localizing properties.

Anionic dodecaborate ($[B_{12}H_{11}]^{2-}$) is one of the most useful boron hydride cage in the syntheses of water soluble and high boron containing compounds for BNCT. Recently, Gabel et al reported the synthesis of racemic dodecaborate-containing α-amino acid having a thiododecaborate (-S-$[B_{12}H_{11}]^{2-}$) unit by forming of boron-sulfur-carbon (-B-S-C-) bonds in the side chain as a new class of boron delivery

agent for BNCT [2]. However, the synthetic method has not been entirely satisfactory, particularly for large scale preparation owing to multiple steps, and for racemic form synthesis. Furthermore, biological activities as boron agent for BNCT has not as yet been reported.

These results prompt us to explore the new synthetic route of optically active thiododecabarate containing amino acid (BSH-amino acid), and to evaluate the biological activities as boron agent. Here, we describe a simple and alternative synthesis of optically active BSH-amino acids **1a-d** and their biological evaluation as boron agentfor BNCT.

Results and Discussion

Synthetic route of four BSH-amino acids (**1a-d**) was illustrated in Fig. 1. Thus, the starting compound, *S*-(cyanoethyl)-BSH tetramethylanmmonium salt (**2**) was prepared in high yield by hetero Michael reaction of BSH dicesium salt with acrylonitrile by using sodium hydroxide as base. On the other hand, *ω*-bromo-L-amino acids (**3a-d**), represented as Br-(CH_2)n-CH(NH_2)COOH (n=1, 2, 3, 6), were prepared as hydrochloric or hydrobromic salts. Among them, (*S*)-2-amino-4-bromobutyric acid (**3b**, n=2) was commercially purchased, and the others (**3a, 3c, 3d**) bearing (*S*)-configuration were synthesized according to the modified literature methods [3], respectively.

The alkylation reaction of **2** with *ω*-bromo-L-amino acids (**3**) was completed by simple procedure as follows; a mixture of **2** and **3** in acetonitrile was refluxed for one day, and then condensed in reduced pressure to give adduct (**4**) as residue, which was used to the next step without further purification. Then, acetone solution of **4** was treated with tetramethylammonium hydroxide (Me_4NOH) in the presence of methylamine to furnish the target amino acid (**1**) in moderate yields. However, in the case of **1a**, the overall yields were poor (21%) due to its lability (Fig. 1). Purity and chemical structure of **1** were analyzed by ^1H and ^{13}C-NMRs, ESI-MS and capillary electrophoresis. In the present synthesis, an absolute configuration of the starting *w*-bromo-L-amino acid is to be introduced to the final amino acids in retention without any racemization.

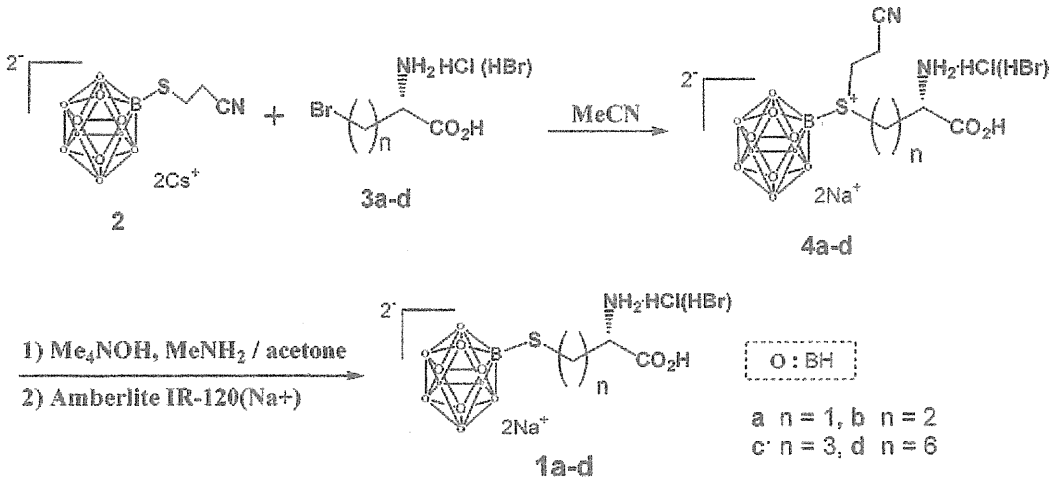

*Fig. 1. Synthesis of Thiododecaborate -Containing L-Amino Acid (BSH-amino acid) (**1a-d**).*

In order to evaluate the uptake of BSH-L-amino acids **1b-d** synthesized here by cancer cells *in vitro*, we measured the boron concentrations in three kinds of cancer cells, C6, B16 SAS by ICP-AES (Fig 2). BSH amino acids **1b, 1c** and **1d** were up-taken in cancer cells. In particular, the boron concentration of **1b-d** are higher than that of L-BPA as of positive control in the case of C6 and B16 cell.

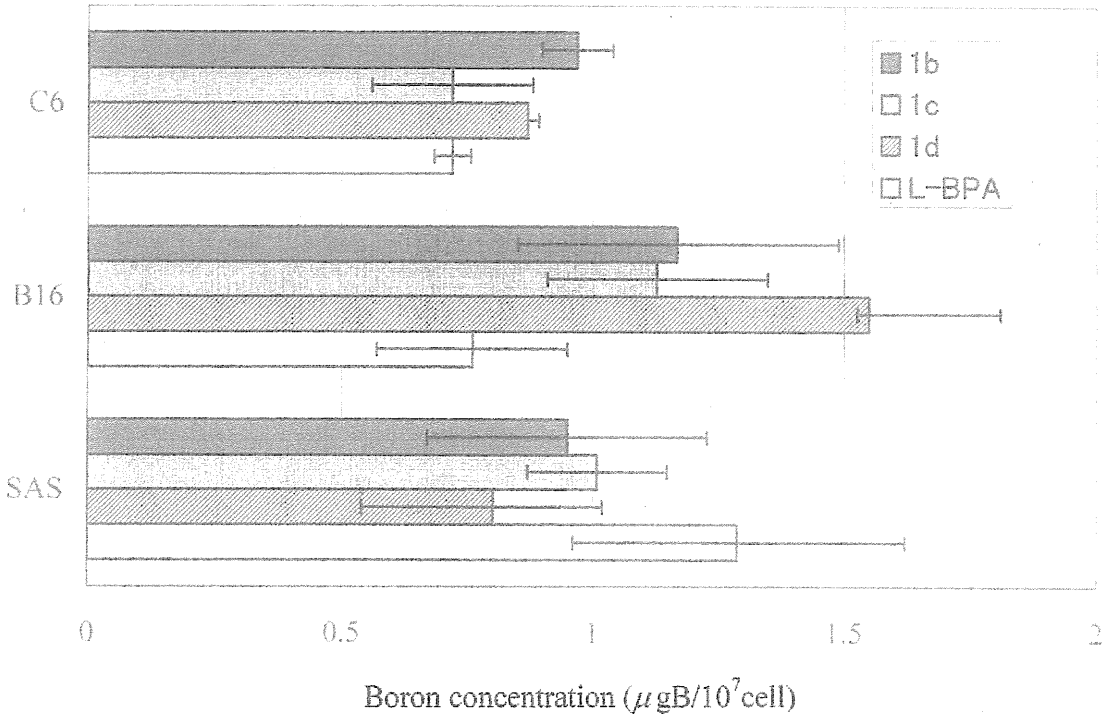

Fig.2. Incorporated amount of boronated amino acids.

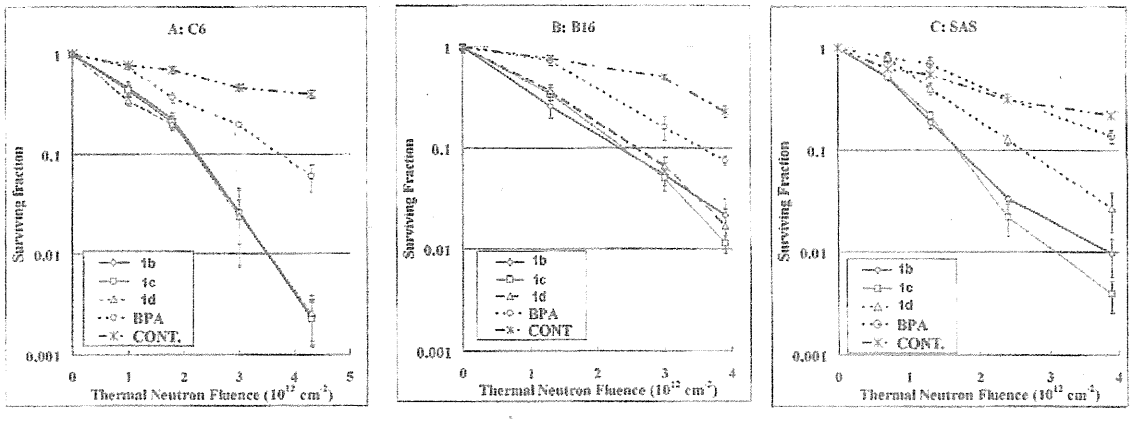

*Fig.3. Tumor cell killing effects of **1b-1d** and BPA. A: against C6 cell. B: against B16 cell. C: against SAS cell.*

Finally, we examined the tumor cell killing effects of **1b-d** against C6, B16 SAS cells in vitro by neutron irradiation (Fig. 3). Despite of the boron concentration of **1b-d** are closely equivalent that of L-BPA, **1b-d** showed higher killing effects than that of L-BPA in the case of each tumor cells.

In conclusion, we have accomplished the efficient and simple synthesis of thiododecaborate-containing L-amino acid (BSH-amino acid) by nearly one-step alkylation of *S*-(cyanoethyl)-BSH with non-protected *ω*-bromo-L-amino acid in moderate yields. We believe that this synthetic method could be applied to another BSH-L-amino acids, such studies are currently in progress. Further biological evaluation *in vivo* is also now under investigation.

References

1. Soloway, A. H.; Tjarks, W.; Barnum, B. A.; Rong, F. G.; Barth, R. F.; Codogni, I. M.; Wilson, J. G. (1998) *Chem. Rev.*, **98**, 1515–1562.
2. Slepukhina I., Gabel D., (2002) *Proceedings of 12th International Congress on Neutron Caputure Therapy*, 247-250.
3. Phadnis, P. P.; Mugesh. G., (2005) *Org. Biomol. Chem.*, **3**, 2476-2481.

Applied Radiation and Isotopes 69 (2011) 1642–1645

Contents lists available at ScienceDirect

Applied Radiation and Isotopes

journal homepage: www.elsevier.com/locate/apradiso

Experimental verification of beam characteristics for cyclotron-based epithermal neutron source (C-BENS)

H. Tanaka [a,*], Y. Sakurai [a], M. Suzuki [a], S. Masunaga [a], T. Mitsumoto [b], K. Fujita [b], G. Kashino [a], Y. Kinashi [a], Y. Liu [a], M. Takada [c], K. Ono [a], A. Maruhashi [a]

[a] Research Reactor Institute, Kyoto University, Osaka 590-0494, Japan
[b] Sumitomo Heavy Industries Ltd., Tokyo 141-6025, Japan
[c] National Institute of Radiological Sciences, Chiba 263-8555, Japan

ARTICLE INFO

Available online 21 March 2011

Keywords:
Boron neutron capture therapy
Cyclotron-based neutron source
Epithermal beam
Multi-foil

ABSTRACT

A cyclotron-based epithermal neutron source has been developed for boron neutron capture therapy. This system consists of a cyclotron accelerator producing 1.1-mA proton beams with an energy of 30 MeV, a beam transport system coupled with a beryllium neutron production target, and a beam-shaping assembly (BSA) with a neutron collimator. In our previous work, the BSA was optimized to obtain sufficient epithermal neutron fluxes of $\sim 10^9$ cm^{-2} s^{-1} using a Monte Carlo simulation code. In order to validate the simulation results, irradiation tests using multi-foil activation at the surface of a gamma-ray shield located behind the collimator and water phantom experiments using a collimated epithermal neutron beam were performed. It was confirmed experimentally that the intensity of the epithermal neutrons was 1.2×10^9 cm^{-2} s^{-1}.

1. Introduction

At the Kyoto University Research Reactor Institute (KURRI), clinical trials of boron neutron capture therapy (BNCT) have been performed using the Kyoto University Research Reactor (KUR) (Sakurai and Kobayashi, 2002). The operation of KUR was stopped from March 2006 to May 2010 because of the change to low-enriched nuclear fuel. Clinical trials were restarted in May 2010.

At KURRI, a cyclotron-based neutron source (C-BENS) has also been developed for clinical use. In our previous work, a beam-shaping assembly (BSA) was optimized to obtain a sufficient intensity of epithermal neutrons, with reduction of gamma-ray contamination and of fast neutron doses (Tanaka et al., 2009). The design-based C-BENS was manufactured and installed at KURRI in December 2008. We started neutron production tests in March 2009. As of December 2010, various irradiation physical characteristics, such as whole-body exposure and measurements of BSA activities for reduction of worker exposure, and also biological characteristics, using cells and mice, had mostly been evaluated. It is especially important to confirm the influence of high-energy neutrons because the neutron energy of the C-BENS is higher than that of KUR.

In this paper, in order to validate the simulation results, irradiation tests using multi-foils for detecting high-energy neutrons over several MeV, and using a water phantom for detecting thermal neutron distributions, were performed.

2. Materials and methods

2.1. Cyclotron-based epithermal neutron source

The C-BENS consists of a cyclotron accelerator, manufactured by Sumitomo Heavy Industries, Ltd. (Tokyo, Japan), which can produce a 1.1-mA proton beam with an energy of 30 MeV, a beam transport system, a BSA, a collimator assembly (CA), and an irradiation bed. A detailed description of the device features is given in Mitsumoto et al. (2010). The schematic layout of the CA and the BSA of the C-BENS is shown in Fig. 1. The CA can move backward to view the setting position of a patient through the collimator window; this backward movement is also used to measure the neutron spectrum under free-in-air conditions in order to establish neutron sources for treatment planning.

To reduce the heat input at the beryllium target, the proton beam was expanded using scanner magnets. Reactions between 30-MeV protons and the beryllium target emit high-energy neutrons, up to 28 MeV, in the 0 degree direction. The BSA can reduce the neutron energy from around 28 MeV to the epithermal energy region because lead and iron work as moderators with inelastic cross-sections, and aluminum and calcium fluoride work as shapers, with a total cross-section, including the valley of

* Corresponding author. Tel.: +81 72 451 2468.
E-mail address: h-tanaka@rri.kyoto-u.ac.jp (H. Tanaka).

0969-8043/$ - see front matter © 2011 Elsevier Ltd. All rights reserved.
doi:10.1016/j.apradiso.2011.03.020

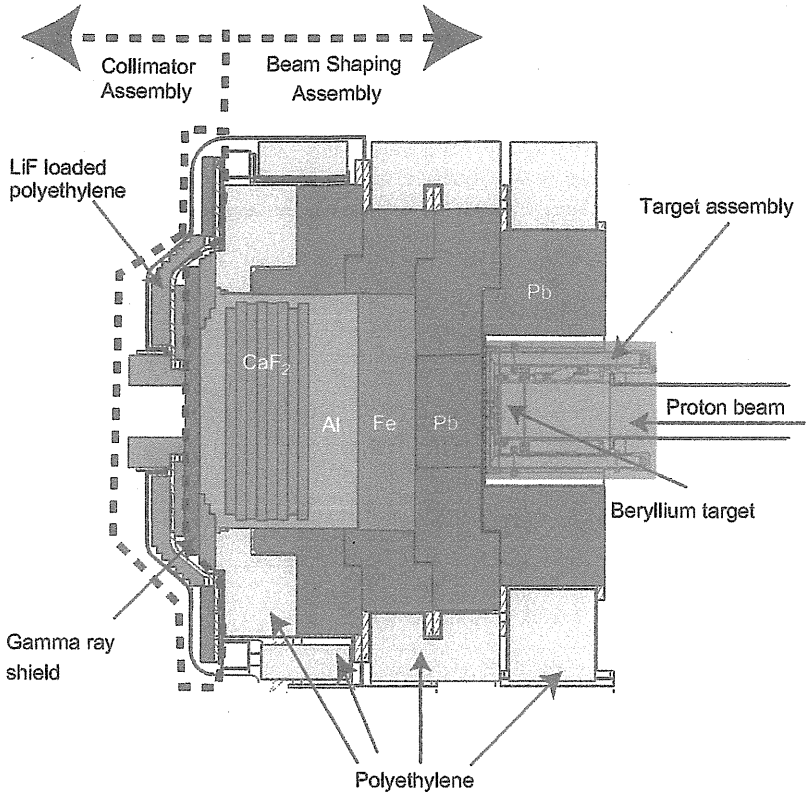

Fig. 1. Schematic layout of the beam-shaping assembly and collimator assembly of a cyclotron-based epithermal neutron source.

several tens of keV. Epithermal neutrons penetrating from the BSA go through a gamma-ray shield.

2.2. Multi-foil measurements

To measure the remaining high-energy neutrons over several MeV, multi-foils such as aluminum, nickel, and iron, which have a threshold energy, were placed at the center of the gamma-ray shield. After irradiation, the activities of the multi-foils were measured by a high-purity germanium detector (HP-Ge). To compare the results with the simulation results obtained with a MCNPX Monte Carlo code, the reaction rates for the multi-foils were derived from the equation below, using corrections such as cooling time: T_c, measuring time: T_m, and irradiation time: T; to correct the irradiation time precisely, variations in the proton current, expressed as $Q_i/\Delta t$, were taken into consideration:

$$R = \frac{\lambda C}{\varepsilon\gamma N_0 e^{-\lambda t_c}(1-e^{-\lambda t_m})\sum_{i=1}^{n}\left(\frac{Q_i}{\Delta t}(1-e^{-\lambda\Delta t})e^{-\lambda(n-i)\Delta t}\right)}, \quad (1)$$

where the constants $\lambda, \varepsilon, \gamma$, and C are the decay constant, detection efficiency, gamma-ray emission ratio, and total photo-peak counts, respectively.

2.3. Water phantom measurements

To measure the dose distributions of thermal neutrons and gamma-rays in a water phantom, a $30 \times 30 \times 20$ cm cubic water phantom was set in front of a collimator of diameter 25 cm. Gold wires and cadmium-covered gold wires were installed at the central axis, to detect thermal neutron flux. TLDs were also set at the central axis. To measure the thermal neutron flux in the lateral direction, gold wires and cadmium-covered gold wires were also installed at depths of 2 and 6 cm. After irradiation, the activities of the gold wires were measured by the HP-Ge. The cadmium ratio was used to estimate the thermal neutron flux.

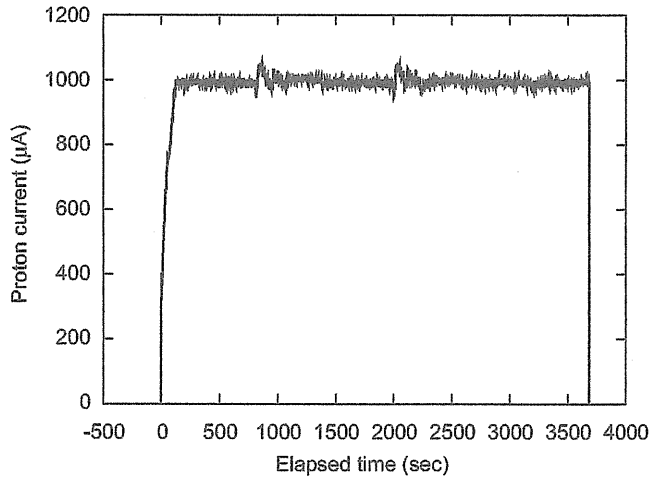

Fig. 2. Relationship between elapsed time and proton current detected at the beryllium target.

3. Results and discussion

3.1. Multi-foil measurements

Fig. 2 shows the typical relationship between elapsed time and proton current at the beryllium target. It was confirmed that the cyclotron can produce a stable proton current of up to ~1 mA for about 1 h. This is enough for use in clinical trials because the

epithermal neutron flux exceeds 10^9 cm^{-2} s^{-1} per proton current of 1 mA.

Fig. 3 shows the ratio of measured reaction rate to calculated reaction rate. Thermal/epithermal neutrons were measured by the reaction of ^{197}Au(n, γ)^{198}Au. To detect high-energy neutrons of the order of MeV, the reactions of ^{58}Ni(n,p)^{58}Co, ^{56}Fe(n,p)^{56}Mn, ^{27}Al(n, α)^{24}Na, and ^{58}Ni(n,2n)^{57}Ni with threshold energies of 2.8, 6.0, 7.2, and 13.5 MeV, respectively, were used. It was found that the ratio of the measured reaction rate to the calculated reaction rate was around 0.7 for the thermal/epithermal and high-energy regions.

According to the reference (Takata, 2010), the neutron spectra for a thick beryllium target using the cross-section data for ENDF/B-VII, and those using experimental data (Brede et al., 1989; Waterman et al., 1979), in the energy range from 17 to 35 MeV, were compared. This revealed that the cross-section data for ENDF/B-VII were higher than the experimental data. The overestimation of the cross-section data for ENDF/B-VII was a factor in the difference between the calculated and measured reaction rates.

Fig. 4 shows the relationship between the proton current at the beryllium target and the measured intensity of the epithermal neutron flux at the surface of a gamma-ray shield. This clearly confirmed good linearity between the proton current and the intensity of the epithermal neutron flux. Hence, the information on the proton current can be used to monitor neutron flux to decide on treatment times. The C-BENS can produce an epithermal flux intensity of up to 1.2×10^9 cm^{-2} s^{-1} with a proton current of 1 mA. In this paper, the energy range from 0.5 to 40 keV was defined as being the epithermal neutron range. The neutron fluxes for the thermal and fast regions were 5.0×10^6 and 6.0×10^7 cm^{-2} s^{-1}, respectively. The dose contaminations per epithermal neutron for fast neutrons and gamma-rays were 5.8×10^{-13} and 7.8×10^{-14} Gy cm^2, respectively.

3.2. Water phantom experiments

Fig. 5 shows the measured thermal neutron distribution in a water phantom compared with the calculated results. The collimator was 25 cm in diameter, which was the maximum size. The calculated

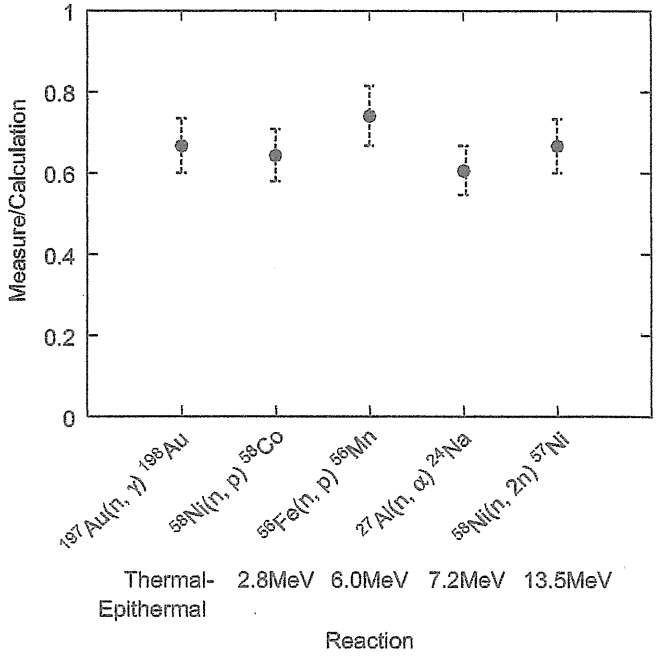

Fig. 3. Ratio of measured data from activities of multi-foils for detecting high-energy neutrons to calculated results using MCNPX.

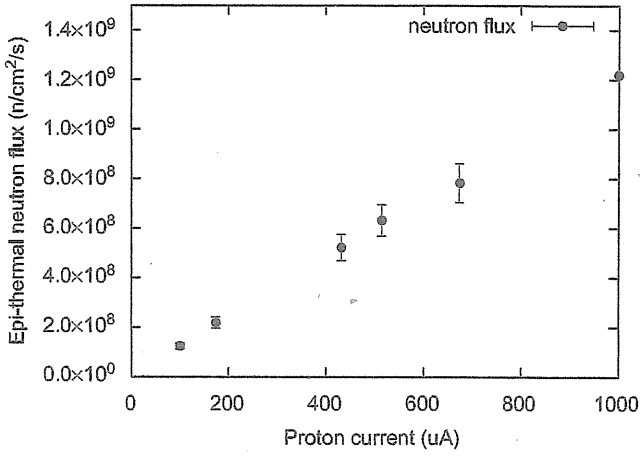

Fig. 4. Relationship between the proton current at the beryllium target and epithermal neutron flux at the surface of the gamma-ray shield.

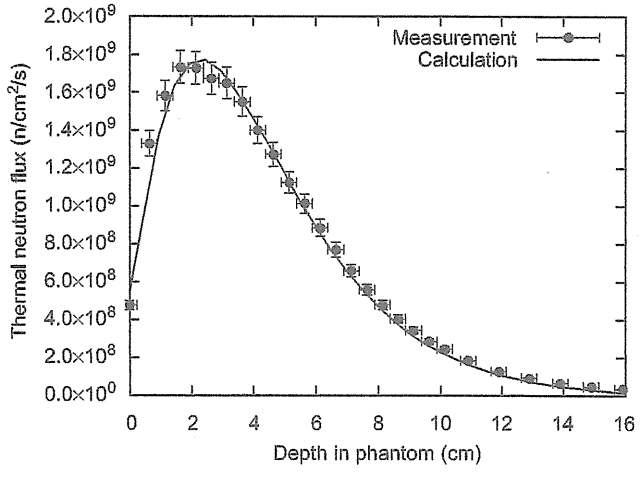

Fig. 5. Thermal neutron distributions in a water phantom at the central axis.

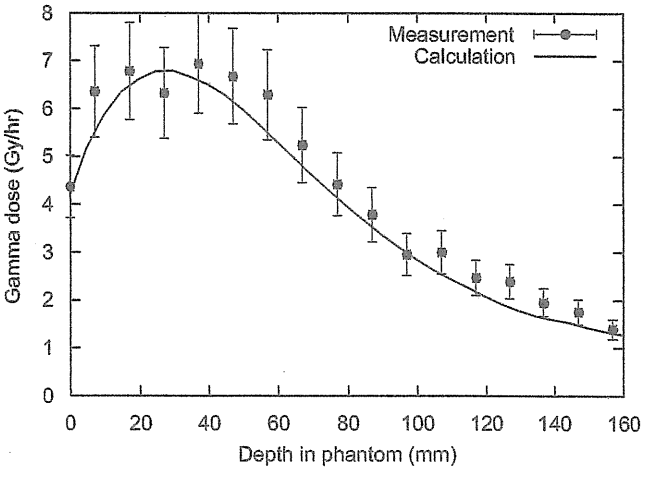

Fig. 6. Gamma-ray dose distributions in a water phantom at the central axis.

results were multiplied by the factor of 0.7 mentioned above. The calculated results multiplied by this factor were in good agreement with the measured data. The thermal neutron flux at a depth of 2 cm was 1.7×10^9 cm^{-2} s^{-1}.

Fig. 6 shows the gamma-ray dose distribution in a water phantom compared with the calculated results. The calculated

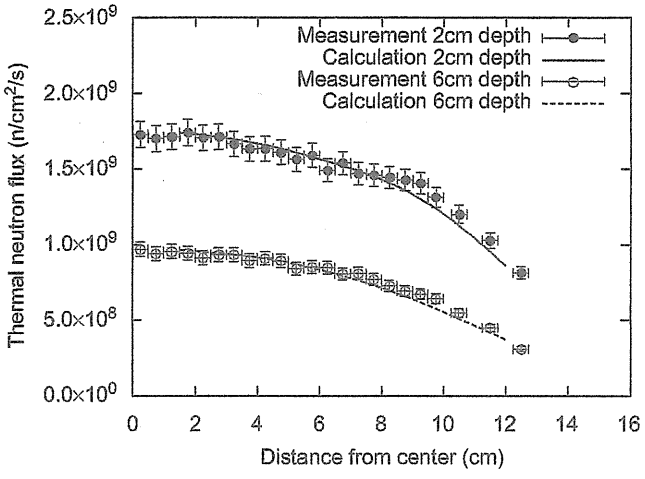

Fig. 7. Thermal neutron distributions in a water phantom in the lateral direction at depths of 2 and 6 cm.

results for the gamma-ray dose were also in good agreement with the measured data, within TLDs errors of less than 15%.

Fig. 7 shows the measured thermal neutron distribution in the lateral direction at depths of 2 and 6 cm. The measured data were also compared with the calculated results multiplied by the factor of 0.7. The calculated results were in good agreement with the measured data, except for distances beyond 8 cm from the center. It was thought that the difference between the measured data and the calculated results beyond 8 cm was caused by the effects of scattering from the walls, floor, and irradiation bed, which were not included in this calculation.

4. Conclusions

Experiments using multi-foils and a water phantom to validate the simulation results obtained with MCNPX code were performed. It was found that the simulation results for reaction rates caused by high-energy neutron and thermal neutron distributions in a water phantom were in good agreement with the measurement results. Good linearity between the proton current and epithermal neutrons at the surface of the gamma-ray shield was confirmed. Hence, the information on proton current can be used for measurements of neutron fluence in the determination of treatment times.

It was found from the experimental results that the intensity of the epithermal neutron flux at the center of the gamma-ray shield was $1.2 \times 10^9\ \mathrm{cm^{-2}\,s^{-1}}$ under proton beam conditions of 1 mA. This value was about twice as large as that for the KUR reactor-based epithermal neutron source, which was used in over 300 clinical trials. Furthermore, C-BENS can produce stable operation with a proton current of 1 mA for 1 h. The use of C-BENS for clinical trials in the near future is desirable.

Acknowledgment

Part of this work was supported by the Association for Nuclear Technology in Medicine, Japan.

References

Brede, H.J., et al., 1989. Neutron yields from thick Be targets bombarded with deutrons and protons. Nucl. Instrum. Methods Phys. Res. A 274, 332–344.

Mitsumoto, T., et al., 2010. Cyclotron-based neutron source for BNCT. In: International Congress on Neutron Capture Therapy, pp. 519–522.

Sakurai, Y., Kobayashi, T., 2002. The medical-irradiation characteristics for neutron capture therapy at the heavy water neutron irradiation facility of Kyoto University Research Reactor. Med. Phys. 29 (10), 2328–2337.

Takata, T., 2010. Study on effective production of accelerator based neutron irradiation field for boron neutron capture therapy, Ph.D. Thesis, Kyoto University.

Tanaka, H., et al., 2009. Characteristics comparison between a cyclotron-based neutron source and KUR-HWNIF for boron neutron capture therapy. Nucl. Instrum. Methods Phys. Res. B 267, 1970–1977.

Waterman, F.M., et al., 1979. Neutron spectra from 35 and 46 MeV protons, 16 and 28 MeV deutrons, and 44 MeV ^{3}He ions on thick beryllium. Med. Phys. 6 (5), 432–435.

Applied Radiation and Isotopes 69 (2011) 1646–1648

Contents lists available at ScienceDirect

Applied Radiation and Isotopes

journal homepage: www.elsevier.com/locate/apradiso

Evaluation for activities of component of Cyclotron-Based Epithermal Neutron Source (C-BENS) and the surface of concrete wall in irradiation room

M. Imoto [a,*], H. Tanaka [b], K. Fujita [c], T. Mitsumoto [c], K. Ono [b], A. Maruhashi [b], Y. Sakurai [b]

[a] Graduate School of Engineering, Kyoto University, Kyoto 606-8501, Japan
[b] Research Reactor Institute, Kyoto University, Osaka 590-0494, Japan
[c] Sumitomo Heavy Industries, Ltd., Tokyo 141-6025, Japan

ARTICLE INFO

Available online 6 April 2011

Keywords:
BNCT
Activity
Identification of radioisotopes

ABSTRACT

The workers employed in BNCT must enter the irradiation room just after an irradiation under the condition of remaining activities. To reduce the radiation exposure for the workers, it is important to identify the origins of the activities. In this research, the activities induced on the concrete wall surface were evaluated using MCNP-5 and the measurement results of thermal neutron distribution. Furthermore, the radioisotopes produced in the moderator were identified with a High Purity Germanium detector. It was found that the activities of the wall were mainly caused by ^{46}Sc, ^{60}Co and ^{152}Eu, and that ^{24}Na and ^{56}Mn were mainly produced in the moderator.

1. Introduction

A new Cyclotron-Based Epithermal Neutron Source (C-BENS) was installed at Kyoto University Research Reactor Institute in December 2008. It was confirmed that the intensity of the epithermal neutron beam was about 1×10^9 cm^{-2} s^{-1}, which could be used for clinical trial of Boron Neutron Capture Therapy (BNCT). Several irradiation experiments for water phantoms, cells and mice are currently underway. To change the irradiation geometries and setups for experiments and/or BNCTs, the workers such as doctors, medical physicists, etc. have to enter the irradiation room under the condition of remaining the activities. It is assumed that the activities are originated from the components of C-BENS and the walls of the irradiation room. To reduce the radiation exposure for the workers, it is important to identify the origins of the activities.

A Monte Carlo simulation was performed to evaluate the thermal neutron distribution in the irradiation room. To confirm the validity of the simulation, the measurement of thermal neutron flux at the surface of the irradiation room was also performed. In addition, the kind of radioisotopes produced in the C-BENS component was experimentally identified using a High Purity Germanium Detector (HPGD).

2. Materials and methods

2.1. Evaluation for the concrete wall

To evaluate radioisotopes produced in the concrete wall, thermal neutron flux distribution was measured by the foil activation method using bare gold foils and cadmium-covered gold foils. The foils were placed on the surface of the concrete wall at intervals of 50 cm, as shown in Fig. 1. After an irradiation for 30 min with a proton current of 1 mA, the activities of gold foils were measured by an HPGD. Using the ratio of the activity between the bare foil and the cadmium-covered foil at the same position, the thermal neutron flux was determined.

The measured fluxes were compared with the calculation results using a Monte Carlo simulation code "MCNP-5" (Sweezy, 2008). In this calculation, the neutron spectrum at the collimator aperture, obtained from the previous work (Tanaka et al., 2009), was used. The F4, which that could derive the neutron spectrum, was placed at the same position as in the experiments. The activities in the concrete were calculated using the thermal neutron fluxes and the cross-section data for the component of the concrete. Table 1 shows the major composition of concrete (Evans et al., 1984). It was assumed that the density of the concrete was 2.1 g cm^{-3}. The cross-section data was obtained from the nuclear data library of ENDF/B-VII (Oblozinsky and Herman, 2006) and "Table of Isotopes" (Firestone, 1996).

In addition, the simulation was also performed in the case of shielding the concrete wall surface to reduce the activities caused by thermal neutrons. We selected a silicone rubber containing 20 wt% B_4C with the thickness of 1 cm as a shielding material.

* Corresponding author. Tel.: +81 72 451 2604.
E-mail address: masayuki.imoto@gmail.com (M. Imoto).

0969-8043/$ - see front matter © 2011 Elsevier Ltd. All rights reserved.
doi:10.1016/j.apradiso.2011.03.018

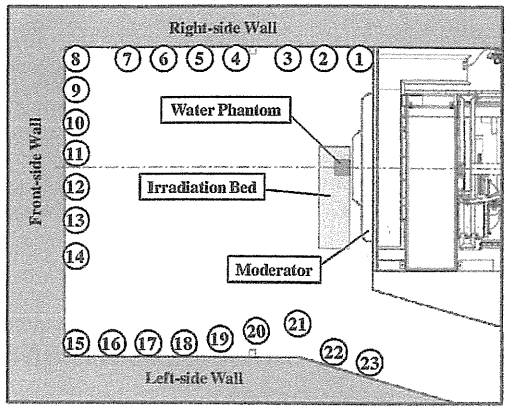

Fig. 1. Schematic layout in the irradiation room for the activation experiments. The numbers represent the positions of the gold foils. A water phantom was placed at the collimator aperture during the irradiation.

Table 1
Major element of concrete. Density of the concrete is assumed to be 2.1 g cm^{-3}.

Element	Composition (ppm)
Si	168,000
Ca	183,000
Sc	6.5
Fe	39,000
Co	9.8
Eu	0.55

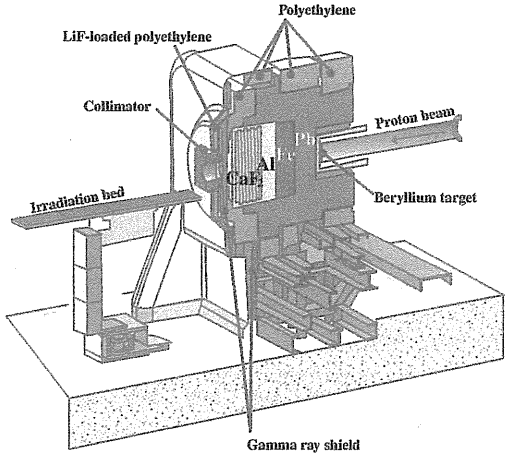

Fig. 2. Schematic layout of the moderator of C-BENS, which is constructed of Fe, Al, CaF_2 and Pb.

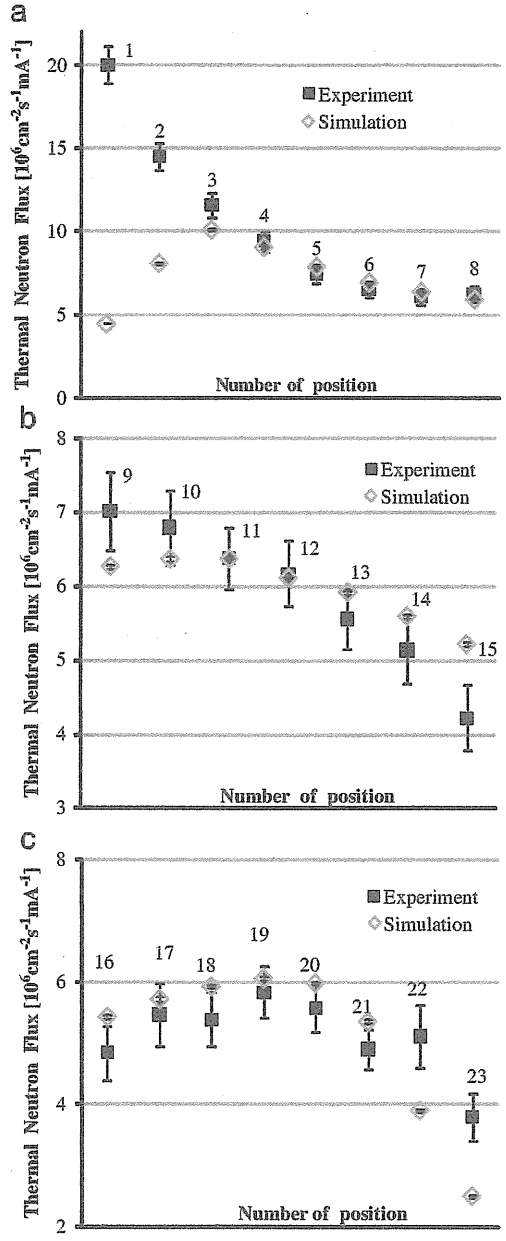

Fig. 3. Comparisons of the thermal neutron distribution on the surface of concrete wall between the calculation results and measured data. The labels represent the position numbers for (a) right-side, (b) front-side and (c) left-side wall.

2.2. Evaluation for the moderator

The kind of the radioisotopes produced in the moderator of the C-BENS was identified using an HPGD. The moderator is constructed of Fe, Al, CaF_2 and Pb as shown in Fig. 2. To prevent the event saturation caused by the background except for the objective, the HPGD was surrounded by gamma-ray shield formed by lead blocks with the collimation of 5 mm^2. The detector was brought into the irradiation room 20 min after an irradiation.

3. Results and discussions

3.1. Evaluation for the concrete wall

The comparisons of the thermal neutron distribution between the calculation results and measured data were shown in Fig. 3. In this figure, the numbers correspond to the evaluation position shown in Fig. 1. The calculation results were in good agreement with the measured data, except for some points. On the right-side wall near the collimator, the measured values were larger than the calculated values. It is suspected that the neutrons generated at the target and the beam line were reflected in the wall and leaked from the gap between the moderator and the concrete walls. This gap should be filled using shielding material such as polyethylene, etc. The calculation result of the thermal neutron flux for the 3rd position was the highest among the evaluation positions except for the leakage from the gap. Hence, the value of thermal neutron flux at the 3rd position was used for calculating the activities of the concrete wall.

Fig. 4 shows the typical neutron spectrum on the surface of concrete wall located at the 3rd and 11th positions. It is clear that thermal neutrons largely contribute to the activation of concrete wall. Based on the operation pattern of the C-BENS, the relationship

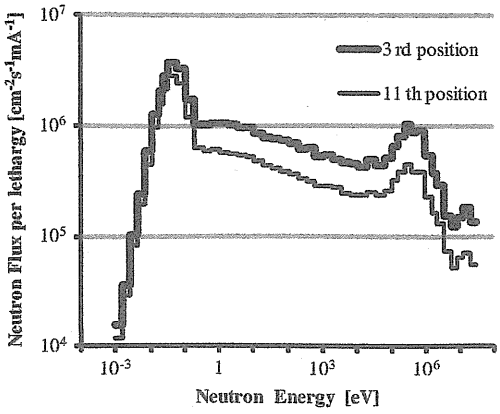

Fig. 4. Typical neutron spectrum on the surface of concrete wall located at the 3rd and 11th positions shown in Fig. 1.

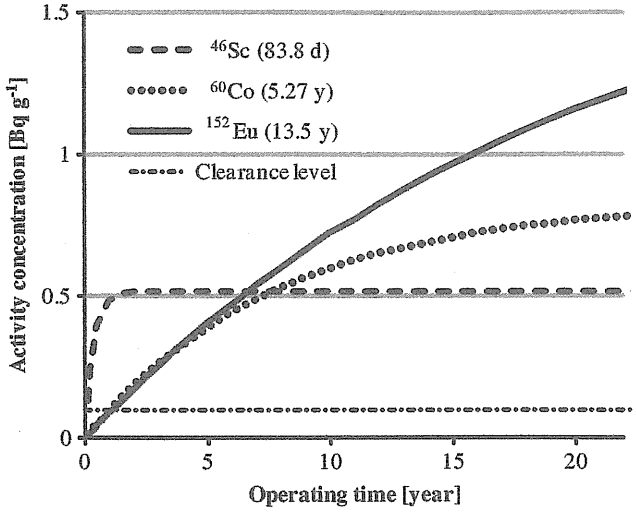

Fig. 5. Relationship between the elapsed time and the activities at the 3rd position located at the right-side wall near the collimator.

between the activities on the surface of concrete wall and elapsed time was estimated. Fig. 5 shows that the activities of the three radioisotopes such as ^{46}Sc, ^{60}Co and ^{152}Eu, exceed the IAEA clearance level of 0.1 Bq g^{-1} in less than 2 years without thermal neutron shield. On the other hand, using a silicone rubber as a thermal neutron shield, we confirmed that the activities of ^{152}Eu could be kept below the clearance level for 10 years, and those of ^{46}Sc and ^{60}Co could be kept below for more than 60 years as shown in Fig. 6.

3.2. Evaluation for the moderator

It was found that most of the activities 20 min after an irradiation were caused by ^{24}Na and ^{56}Mn. These radioisotopes can be generated from ^{27}Al(n,α)^{24}Na or ^{23}Na(n,γ)^{24}Na and ^{56}Fe(n,p)^{56}Mn or ^{55}Mn(n,γ)^{56}Mn. The isotopes such as ^{23}Na and ^{55}Mn are included in the component of C-BENS, just as impurity elements. The moderator of C-BENS consists of lead, iron, aluminum and calcium fluoride, and the isotopes such as ^{27}Al and ^{56}Fe are abundantly included. Therefore, it was concluded that the

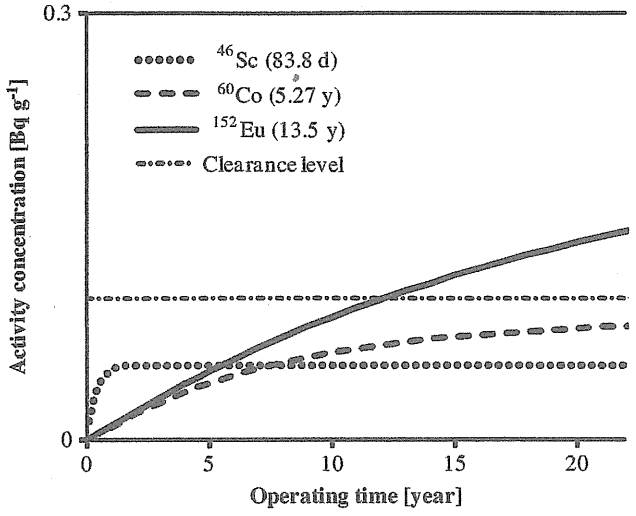

Fig. 6. Relationship between the elapsed time and the activities at the 3rd position located at the right-side wall near the collimator using thermal neutron shield.

radioisotopes such as ^{24}Na and ^{56}Mn were produced mainly due to the reactions such as ^{27}Al(n,α)^{24}Na and ^{56}Fe(n,p)^{56}Mn, respectively.

4. Conclusions

The activities induced at the surface of concrete wall of BNCT irradiation room were evaluated. Thermal neutron flux at the surface of concrete wall was determined by the gold foil activation method and simulation using MCNP-5. The activities were calculated using the cross-section data of ENDF/B-VII and the composition data of concrete. It was shown that the activities will exceed the IAEA clearance level of 0.1 Bq g^{-1} in less than 2 years without thermal neutron shield. However, the activities would have been below the clearance level for 10 years if the wall surface was shielded by silicone rubber containing 20 wt% B_4C with the thickness of 1 cm.

The kind of radioisotopes produced in the moderator of the C-BENS was identified using an HPGD surrounded by lead gamma-ray shield. It was found that most of the activities 20 min after an irradiation were caused by ^{27}Al(n,α)^{24}Na and ^{56}Fe(n,p)^{56}Mn. We found that the activities of the component of C-BENS were much higher than that of the concrete wall and these influence a radiation exposure for the workers. In the future work, quantitative estimation of the activities of the moderator of C-BENS will be performed.

References

Evans, J.C., et al., 1984. Long-Lived Activation Products in Reactor Materials. Nureg/CR, 3474.
Firestone, R.B., 1996. Table of Isotopes. eighth ed. In: Singh, B. (Ed.), Table of Isotope Data, vol. II. John Wiley & Sons, Inc., New York, p. 1554.
Oblozinsky, P., Herman, M., 2006. Evaluated Nuclear Data file ENDF/B-VII.0. Nuclear Data Sheets vol. 107 (issue 12), 2931–3118.
Sweezy, Jeremy E., 2008. MCNP—A General Monte Carlo N-Particle Transport Code, Version 5.
Tanaka, H., et al., 2009. Characteristics comparison between a cyclotron-based neutron source and KUR-HWNIF for boron neutron capture therapy. Nuclear Instruments and Methods in Physics Research B 267, 1970–1977.

Applied Radiation and Isotopes 69 (2011) 1657–1659

Contents lists available at ScienceDirect

Applied Radiation and Isotopes

journal homepage: www.elsevier.com/locate/apradiso

The optimization study of Bonner sphere in the epi-thermal neutron irradiation field for BNCT

H. Ueda [a,*], H. Tanaka [b], A. Maruhashi [b], K. Ono [b], Y. Sakurai [b]

[a] Department of Nuclear Engineering, Kyoto University, Yoshida Honmachi, Sakyo-ku, Kyoto 606-8501, Japan
[b] Research Reactor Institute, Kyoto University, Asashiro-nishi 2-1010, Kumatori-cho, Osaka 590-0494, Japan

ARTICLE INFO

Available online 2 February 2011

Keywords:
Bonner sphere
Epi-thermal neutron irradiation field
Spectrum measurement
Boric acid solution

ABSTRACT

The optimization study on the Bonner sphere in the epi-thermal neutron irradiation field for BNCT was done for the moderator material, moderator size, and activation foils as a neutron detector in the sphere. The saturated activity for the activation foil was obtained from the calculated response, and the effective energy range for each Bonner sphere was determined from the saturated activity. We can see that boric acid solution moderator is suitable for the spectrum measurement of a epi-thermal neutron irradiation field.

1. Introduction

The neutron energy of epi-thermal neutron irradiation field for BNCT covers a wide energy range. It is necessary to evaluate the neutron dose for a certain neutron-energy, because the physical property and the biological effectiveness greatly vary according to the neutron energy. Thereby, it is important to obtain the detailed information for the neutron energy spectrum before the clinical use.

In Kyoto University Research Reactor Institute (KURRI), a new BNCT irradiation system, Cyclotron-Based Epithermal Neutron Source (C-BENS), was installed in December 2008 (Tanaka et al., 2009). The several evaluations for the irradiation characteristics of this system are currently underway.

The Bonner-sphere method is one of the effective methods for the detailed evaluation of neutron energy spectrum. This method is applied for the spectral evaluation of C-BENS. Some activation foils are used as the neutron detector, and some neutron moderators are used as the sphere-wall material. For the optimization of Bonner sphere, simulation calculations for the Bonner sphere response were performed. In this paper, the optimization study on the Bonner sphere is reported.

2. Materials and methods

2.1. Bonner sphere

Bonner sphere consists of a spherical neutron-moderator shell and neutron detector placed in the sphere center. The incident epi-thermal neutron on a Bonner sphere is moderated through the moderator to thermal neutron, which is easy to detect by a kind of neutron detectors. Using the various sizes of Bonner spheres, it is possible to determine the detailed neutron spectra for the wider energy range.

In this study, activation foil was used as a neutron detector for the Bonner sphere. Indium (In), gold (Au), manganese (Mn), copper (Cu) and iron (Fe) were selected as the activation-foil materials. Water, water including boron-10, polyethylene, and graphite were selected as the neutron moderators, and the sphere diameters were changed from 5 to 20 cm for 5-cm increments. These optimized combinations were determined for the epi-thermal neutron irradiation field.

The specific saturated activity A_i^{nucl} [$g^{-1}\,s^{-1}$] using the i-th Bonner sphere is obtained from the measurement data. The superscript *nucl* represents the nuclide activated in the activation-foil, such as ^{197}Au, ^{63}Cu, etc. The saturated activity is approximately expressed in the following equation:

$$A_i^{nucl} = \sum_j R_{ij}^{nucl} \phi_i \quad (1)$$

where ϕ_i [$cm^{-2}\,s^{-1}$] is neutron flux for the j-th energy group, and R_{ij}^{nucl} [$cm^2\,g^{-1}$] is the response of the activated nuclide in unit mass of activation foil to neutron flux of the jth energy group (Awschalom and Sanna, 1985).

2.2. Irradiation system

The neutron energy spectra of the C-BENS irradiation system were calculated for some annular sources for the beam centerline. The calculated spectra are shown in Fig. 1. The vertical axis corresponds to neutron flux per a cyclotron beam-current at 1 mA. In the optimizing simulation, the spectrum in the annulus

* Corresponding author. Tel./fax: +81 72 451 2604.
E-mail address: haruaki@physics.mbox.media.kyoto-u.ac.jp (H. Ueda).

0969-8043/$ - see front matter © 2011 Elsevier Ltd. All rights reserved.
doi:10.1016/j.apradiso.2011.01.034

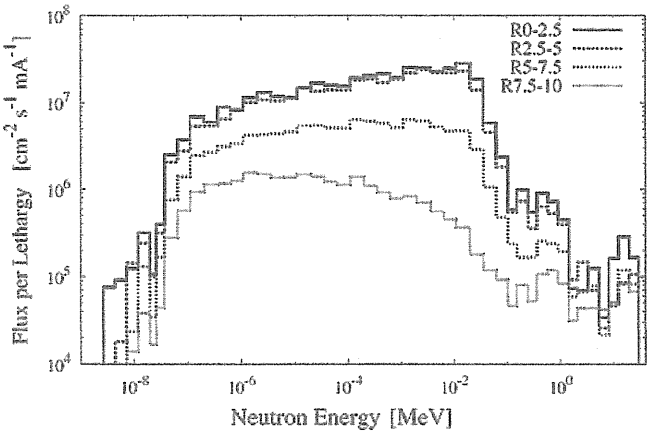

Fig. 1. Energy spectra of the epi-thermal neutron beam of C-BENS using 5-cm-radius collimator aperture. "R0-2.5" represents the annulus of 0-cm inner-radius and 2.5-cm radius.

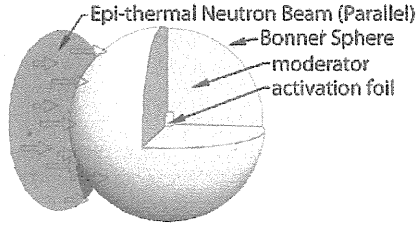

Fig. 2. Calculation geometry for the Bonner sphere response.

R0-2.5 of 0-cm inner-radius and 2.5-cm outer-radius, namely the circle of 2.5-cm radius, was considered as the representative spectrum for the C-BENS irradiation system.

2.3. Optimization of Bonner sphere

The survey calculations were performed for the responses, R_{ij}^{nucl}, for the combinations of the foils, the moderators and the sphere diameters. In the calculations, a Monte Carlo simulation code MCNP-4C2 was used (Breismeister, 2000). The calculation geometry is shown in Fig. 2. It was assumed that the directionality of the epi-thermal neutron beam was parallel and the intensity distribution on the source surface was homogeneous. The saturated activity for the C-BENS irradiation system was calculated for each energy bin, using the obtained response. The optimized energy range for each Bonner sphere was decided.

3. Results and discussions

3.1. Optimized combinations of Bonner sphere

The calculated normalized responses of ^{197}Au for the Bonner sphere using every moderator material are shown in Figs. 3–8. The saturated-activities of ^{197}Au for the C-BENS irradiation system, calculated on the assumption of the R0-2.5 spectra, are shown in Fig. 9.

On the optimization, two following points were considered. First, from Eq. (1), it is better to use the various Bonner spheres with the different normalized response functions ($R_{ij}^{nucl}/\sum_j R_{ij}^{nucl}$) for the neutron detection of the wider energy range. Second, the Bonner sphere is unavailable for the measurement of the energy range in which the saturated activity is too low to be submerged by the error. For example, in Fig. 9, 20-cm-diameter Bonner sphere using water including ^{10}B of 1 wt% is useful for higher energy region measurement, not for lower.

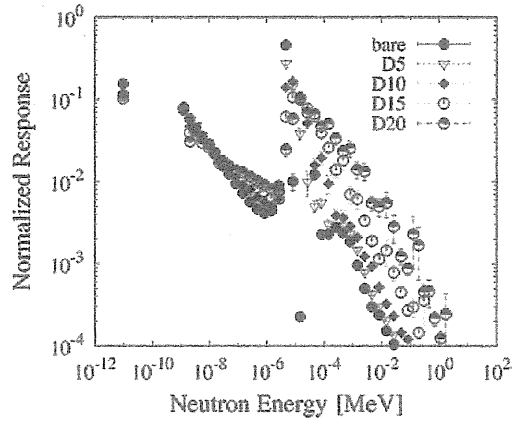

Fig. 3. Calculated normalized responses of ^{197}Au for the Bonner sphere using graphite. "D10" represents the 10 cm-diameter Bonner sphere, and "bare" corresponds to the case without the moderator sphere.

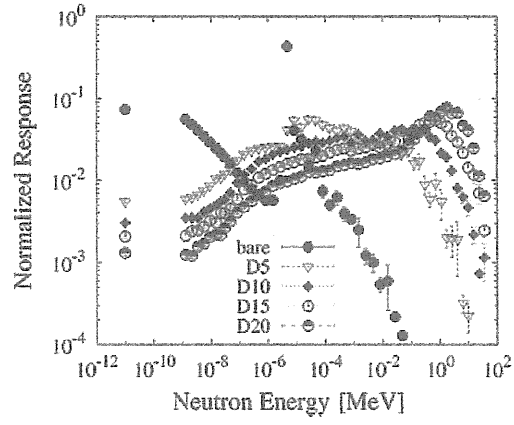

Fig. 4. Calculated normalized responses of ^{197}Au for the Bonner sphere using polyethylene.

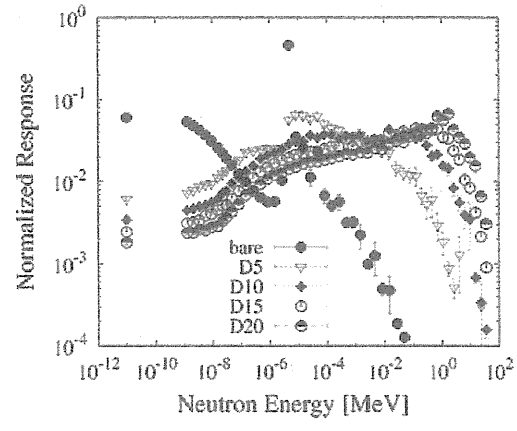

Fig. 5. Calculated normalized responses of ^{197}Au for the Bonner sphere using water.

According to these points, the combinations of the Bonner sphere were determined for the neutron energy region. The response functions for the following three moderators, such as water, polyethylene, and boric acid solution with boron-10 of less than 0.1 wt%, were very similar. It was considered that the Bonner spheres with these moderators make almost the same response.

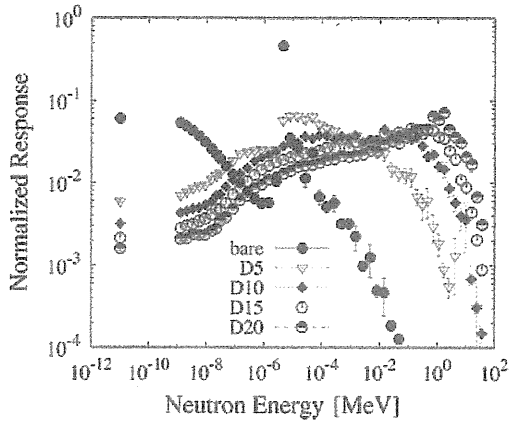

Fig. 6. Calculated normalized responses of ^{197}Au for the Bonner sphere using water including ^{10}B of 0.01 wt%.

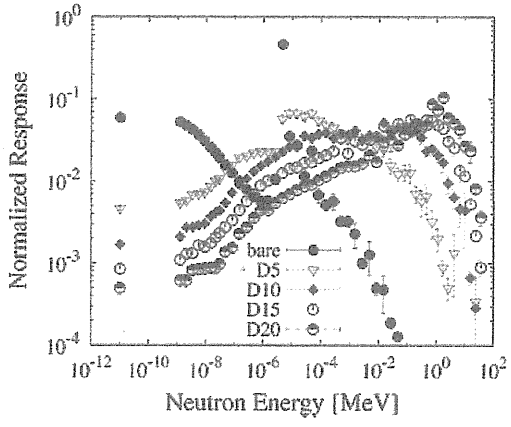

Fig. 7. Calculated normalized responses of ^{197}Au for the Bonner sphere using water including ^{10}B of 0.1 wt%.

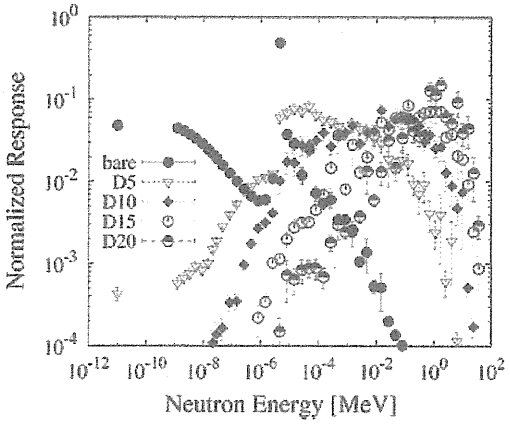

Fig. 8. Calculated normalized responses of ^{197}Au for the Bonner sphere using water including ^{10}B of 1 wt%.

The optimized combinations for the three neutron-energy-regions, such as thermal (−0.5 eV), epi-thermal (0.5 eV 40 keV) and fast neutron-regions (40 keV), are as follows.

As the moderator material, water and/or boric acid solution with boron-10 of more than 0.1 wt% are suitable for the three neutron-energy-regions. For the activation foil, Mn, Cu and/or Fe are suitable for the thermal neutron region, and In, Au, Mn, Cu and Fe are suitable for the epi-thermal neutron region. For the fast neutron region, it is the most suitable activation foil, as the threshold reaction of 115In(n, n)115*In, can be applied.

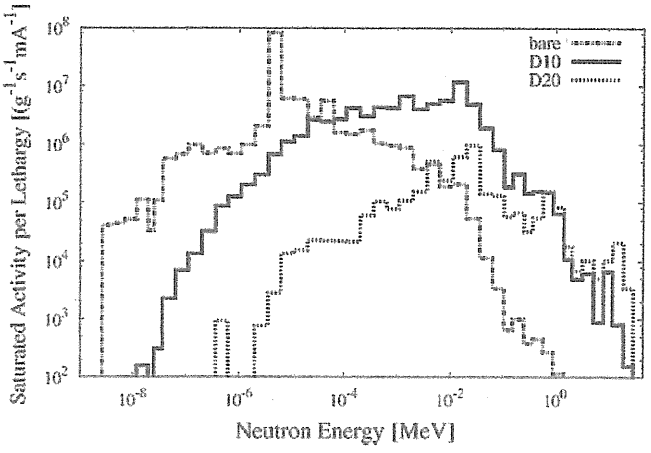

Fig. 9. The saturated-activities of ^{197}Au, calculated on the assumption of the RO-2.5 spectra, for the Bonner sphere using water including ^{10}B of 1 wt%. "D10" represents the 10-cm-diameter Bonner sphere, and "bare" corresponding to the case without the sphere.

3.2. Boric acid solution moderator

In this study, we found that boric acid solution with ^{10}B of more than 0.1 wt% is suitable moderator material for the wide energy range measurement. We can easily change the response function of Bonner sphere with the various concentrations of boric acid solution moderator. Boric acid solubility is 47.2 g/l at 20 °C (IUCLID Dataset, 2000). It corresponds to boric acid solution with ^{10}B of about 0.15 wt%. But, we can increase weight percent of ^{10}B with ^{10}B enrichment of natural boron.

4. Conclusions

The optimized combination for the Bonner sphere was determined for the spectral evaluation of the C-BENS neutron beam. For the evaluation in the thermal neutron energy range, Mn, Cu and Fe are suitable as the activation foil. For the evaluation in the epi-thermal range and higher energy range to 1 MeV, water moderator with the diameter of more than 20 cm is suited. And, each of the activation foils of In, Au, Mn, Cu and Fe can be used. Boric acid solution is suitable as the moderator for the wide energy range. Especially, responses of Bonner spheres with boric acid solution moderator are easy to change increasing ^{10}B concentration.

References

Awschalom, M., Sanna, R., 1985. Applications of Bonner Sphere Detectors in Neutron Field Dosimetry. Radiat. Prot. Dosimetry 10, 89–101.

Breismeister, F., 2000. MCNP—A General Monte Carlo N-Particle Transport Code. Version 4C, LA-13709-M. Los Alamos National Laboratory.

IUCLID Dataset, 2000. Boric acid, crude natural, containing not more than 85 per cent of H3BO3 calculated on the dry weight. 10043-35-3. European Commission, European Chemicals Bureau.

Tanaka, H., Sakurai, Y., Suzuki, M., Takata, T., Masunaga, S., Kinashi, Y., Kashino, G., Liu, Y., Mitsumoto, T., Yajima, S., Tsutsui, H., Takada, M., Maruhashi, A., Ono, K., 2009. Improvement of dose distribution in phantom by using epithermal neutron source based on the be (p,n) reaction using a 30 MeV proton cyclotron accelerator. Applied Radiation and Isotopes 67, S258–S261 13th International Congress on Neutron Capture Therapy BNCT: A New Option Against Cancer.

Applied Radiation and Isotopes 69 (2011) 1830–1833

Contents lists available at ScienceDirect

Applied Radiation and Isotopes

journal homepage: www.elsevier.com/locate/apradiso

A phantom experiment for the evaluation of whole body exposure during BNCT using cyclotron-based epithermal neutron source (C-BENS)

T. Tsukamoto [a,*], H. Tanaka [b], H. Yoshinaga [b], T. Mitsumoto [c], A. Maruhashi [b], K. Ono [b], Y. Sakurai [b]

[a] Graduate School of Engineering, Kyoto University, Yoshida Honmachi, Sakyo-ku, Kyoto 606-8501, Japan
[b] Research Reactor Institute, Kyoto University, Asashiro-nishi 2-1010, Kumatori-cho, Osaka 590-0494, Japan
[c] Sumitomo Heavy Industries, Ltd., Osaki 2-1-1, Shinagawa, Tokyo 141-6025, Japan

ARTICLE INFO

Available online 21 March 2011

Keywords:
Cyclotron-based epithermal neutron source
Whole body exposure
Water phantom
Dose equivalent

ABSTRACT

At Kyoto University Research Reactor Institute (KURRI), cyclotron-based epithermal neutron source was installed in December 2008, and the supplementary construction works have been performed. As of December 2010, the various irradiation characteristics important for BNCT were mostly evaluated. The whole body exposure during BNCT medical irradiation is one of the important characteristics.

In this article, measurements of absorbed dose for thermal and fast neutrons and gamma-ray at ten positions corresponding to important organs are reported.

1. Introduction

At KURRI, cyclotron-based epithermal neutron source (C-BENS) was installed in December 2008, and neutron generation test was begun in March 2009. C-BENS consists of a cyclotron accelerator that can produce 1 mA, 30 MeV protons, a beam transport system with a neutron production beryllium target and the moderator for reducing the neutron energy from high energy up to 28 MeV to epithermal energy (Tanaka et al., 2009a). As of December 2010, the various irradiation characteristics important for BNCT, physical characteristics test and biological characteristics test using cell and mice were mostly evaluated. It was confirmed that the epithermal neutron beam intensity is about twice larger than that of heavy water neutron irradiation facility (HWNIF) of Kyoto University Reactor (KUR) (Sakurai and Kobayashi , 2002). However, fast neutron energy generated by beryllium target of C-BENS was higher than that of HWNIF. Hence, it is necessary to evaluate the whole body exposure caused by fast neutrons during medical BNCT irradiation.

To experimentally evaluate absorbed dose in whole human body, a water-filled phantom modified for whole human body was prepared. The measurements of thermal and fast neutron flux using neutron activation foils, and gamma-ray dose using thermo-luminescent dosimeters (TLDs) were performed. In this article, the evaluations of absorbed dose based on the measurement results at the locations of important organs are reported.

2. Material and methods

2.1. A human whole-body phantom

The human whole-body phantom is 170 cm in height, and consists of some rectangular acrylic-resin cases filled with water as shown in Fig. 1.

Thermal neutron flux was measured with neutron activation foil method using bare gold foils and cadmium-covered gold foils. The gold foils are 10 mm in diameter with the thickness of 0.05 mm. The fast neutron flux over the energy of 0.5 MeV was determined with the activity of indium foils. The indium foils are 20 mm in diameter with the thickness of 0.10 mm. Gamma-ray dose was measured by using TLDs. TLDs were made of beryllium oxide sealing in quartz cell in order to reduce the sensitivity for neutrons. The gold foils and TLDs were placed at ten positions: (1) brain, (2) thyroid, (3) esophagus, (4) bone marrow, (5) lung, (6) stomach, (7) liver, (8) colon, (9) bladder and (10) gonad. And the indium foils were positioned at nine positions except for the brain.

For the irradiation tests, it was assumed that a target volume was positioned at the depth of 2 cm from the left lateral surface of the head phantom and irradiated in the supine position. The phantom was attached to the beam aperture and the schematic layout of this experiment is shown in Fig. 2. The shape of the beam is circular and the size of irradiation field is 10 cm in diameter. After the irradiation, the activities of the gold and indium foils were measured with high-purity germanium detector (model GEM20P4, ORTEC).

2.2. Evaluation of the absorbed dose

In order to calculate the absorbed dose at ten positions, the neutron and gamma-ray sources at the surface of collimator,

* Corresponding author. Tel./fax: +81 72 451 2604.
E-mail addresses: t.tsukamoto@ft5.ecs.kyoto-u.ac.jp, tsukamoto3251@gmail.com (T. Tsukamoto).

0969-8043/$ - see front matter © 2011 Elsevier Ltd. All rights reserved.
doi:10.1016/j.apradiso.2011.03.013

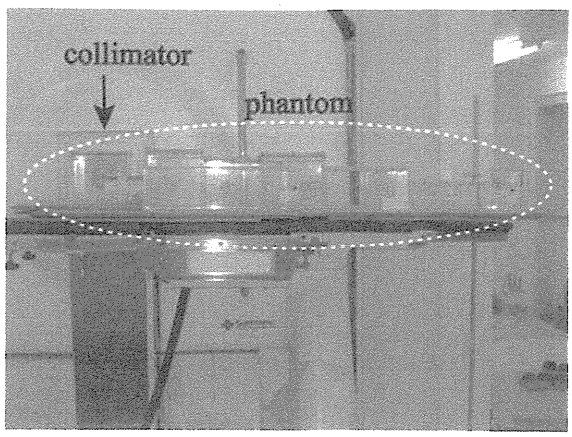

Fig. 1. Photograph of the experiments using a human whole-body phantom.

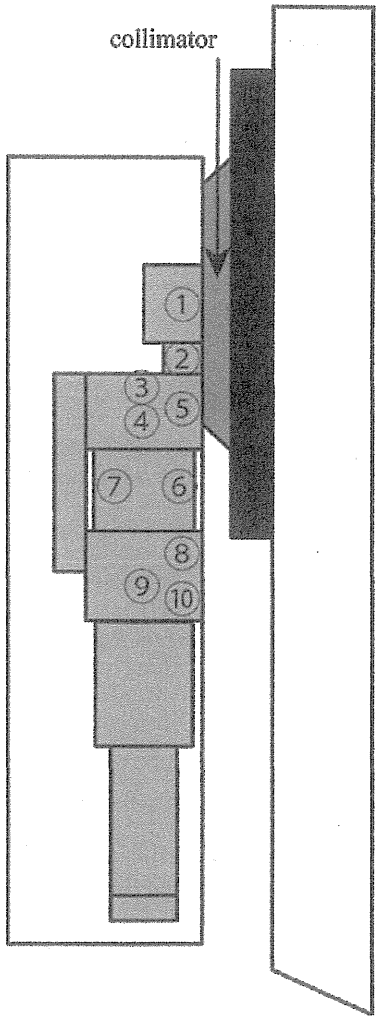

Fig. 2. Schematic layout of the irradiation tests in the supine position using a whole-body phantom. The numbers represent the assumed important organs 1, head; 2, thyroid; 3, esophagus; 4, bone marrow; 5, lung; 6, stomach; 7, liver; 8, colon; 9, bladder; and 10, gonad.

which were estimated by previous work (Tanaka et al., 2009a), were used. In the calculation, the collimator structures were modeled and the sources were modeled up to 150 cm in radius. The typical neutron spectra near the organs such as head, lung and liver are shown in Fig. 3. The calculated thermal and fast neutron absorbed doses were derived from the multiplication between the neutron spectrum calculated by MCNPX and kerma factors (Chadwick et al., 1999) considering the elemental components of each organ (ICRU, 1992).

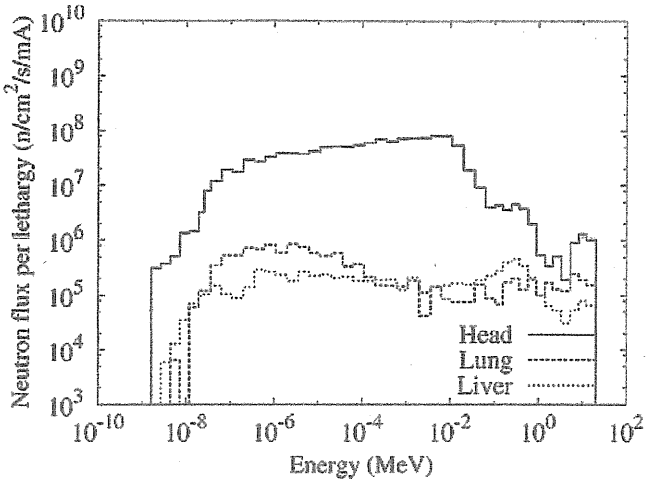

Fig. 3. Typical neutron energy spectra on the surface of head, and near lung and liver.

2.2.1. Absorbed dose for thermal neutrons

The calculated data of absorbed dose for thermal neutrons at each organ is normalized with the ratio of the measured and calculated data at the peak of the thermal neutron flux distribution in the head phantom. In this experiment, the activity at the peak of the thermal neutron distribution is highest compared with other position. Therefore, it is easy to obtain less statistical error. We select the location at the peak position to normalize.

On the other hand, to estimate the measured absorbed dose due to thermal neutrons, the calculated absorbed dose data was multiplied with the measured-to-calculated thermal neutron flux ratio.

2.2.2. Absorbed dose for fast neutrons

The calculated fast neutron absorbed dose at each organ is normalized with the ratio of the measured-to-calculated indium reaction rate at the position of thyroid in the neck phantom. In this experiment, the activity at the thyroid is highest compared with other position. Therefore, it is easy to obtain less statistical error. We select the location at the position of thyroid to normalize. The calculated reaction rate was derived from the multiplication of the energy spectrum and the cross-section data of JENDL/D-99.

On the other hand, to estimate the measured fast neutron absorbed dose, the calculated absorbed dose data was multiplied with the measured-to-calculated indium reaction rate ratio.

2.2.3. Gamma-ray dose

In order to estimate primary gamma-rays generated from the C-BENS components and secondary gamma-rays caused by the reactions between the neutrons and human body elements such as hydrogen, the calculations using F4 tally of MCNPX code without electron transport were performed separately with the neutron and gamma-ray sources. To derive the gamma ray dose, the flux to dose conversion factor was used. The measured primary and secondary gamma-ray doses are estimated by using the primary-to-secondary gamma-ray dose ratio calculated with